CLM - P 550

CLM - P 550

UKAEA

Preprint

CLASSIFICATION OF X-RAY SPECTRA OF 2-3 TRANSITIONS IN THE Ne-LIKE AND Na-LIKE ISOELECTRONIC SEQUENCES OF THE ELEMENTS FROM KRYPTON TO MOLYBDENUM

H GORDON
M G HOBBY
N J PEACOCK
R D COWAN

CULHAM LABORATORY
Abingdon Oxfordshire

1979

CLM-P550

CLASSIFICATION OF X-RAY SPECTRA OF 2-3 TRANSITIONS IN THE Ne-LIKE AND Na-LIKE ISOELECTRONIC SEQUENCES OF THE ELEMENTS FROM KRYPTON TO MOLYBDENUM

by

H Gordon [+], M G Hobby, N J Peacock and R D Cowan [x]

Culham Laboratory, Abingdon, Oxon OX14 3DB, UK
(Euratom/UKAEA Fusion Association)

ABSTRACT

Plasmas produced by the laser irradiation of solid targets and in a Plasma Focus device have been employed as sources of X-ray spectra of the elements Kr(Z=36) - Mo(Z=42). The Ne-like isoelectronic sequence has been investigated by comparing observed wavelengths with ab initio atomic structure calculations and isoelectronic interpolation. Previous identifications in Ne-like ions have been extended to krypton, rubidium and strontium. The Na-like satellite structure of these elements has also been studied and a detailed classification of these satellites is presented.

(Submitted for publication in J.Phys.B., Atom. Molec.Phys.

[x]The University of California, Los Alamos Scientific Laboratory, Los Alamos, New Mexico, 87545, USA

+On attachment from the University of Essex

AUGUST 1978

CMS

1. INTRODUCTION

Interest in the spectroscopy of highly stripped ions has grown as a result of its unique role in the determination of plasma parameters in the high density plasmas produced by the irradiation of solid targets (Peacock 1977, Hughes 1975). Term scheme classification is also relevant to the study of elements of interest in astrophysical plasmas (Pye et al 1977) and Tokamak fusion research (Breton et al 1978). In Tokamaks for example, elements such as molybdenum, from current aperture limiters, appear as impurities in the hydrogen discharge and dramatically affect the overall energy balance of these plasmas through their contribution to radiative cooling. Recent reports have included the observation of Mg-, Na- and Ne-like ions of molybdenum from Tokamaks (Schwob 1977, Hinnov 1976). The projected use of elements such as zirconium and niobium in the fabrication of such devices (Hotston 1978) and the conceivable need to introduce rare gases such as krypton for diagnostic purposes make it imperative that the unambiguous identification of these elements is obtained. Of particular interest are the spectra of Ne-like ions and their satellites since there is the possibility of using them for diagnostic purposes (Burkhalter et al 1975). These ions have a closed shell configuration and are particularly persistent in plasmas.

The laser produced spectra of highly ionised molybdenum below 10 Å has been observed by Aglitskii et al (1975) who included yttrium, zirconium and niobium in an analysis of the Ne-like isoelectronic sequence. More recently molybdenum spectra in the wavelength region 10 - 200 Å has been classified by Mansfield et al (1978) and Burkhalter et al (1977) and includes data up to Mo XXXII (Na-like). Burkhalter et al have also published a study of the Ne-like isoelectronic sequence of Zn, Br, Se, Ge and Zr together with some interpretation of their Mg- and Na-like satellites. A useful survey of the X-ray spectroscopy of multiply-charged ions from laser produced plasmas has been published by Boiko et al (1978) where many members of the Ne-like isoelectronic sequence are classified or predicted. The present paper extends the classification of the X-ray spectra of 2 - 3 transitions from Ne-like ions to Kr, Rb and Sr and presents a detailed classification of the Na-like satellites of highly ionised krypton to molybdenum.

2. EXPERIMENTAL

A spectrum of krypton was observed in the transient pinch occurring in a coaxial plasma gun device known as the Plasma Focus. This device is described more fully elsewhere (Peacock et al 1969). The plasma is produced using a

static gas filling of D_2 doped with a few percent of gas impurities, in this case krypton and argon, the H- and He-like lines of argon (Peacock et al 1969) being used as calibration wavelengths for the krypton spectrum.

The spectra of rubidium to molybdenum were recorded from laser produced plasmas. These plasmas were produced by focusing the output of a multi-gigawat Nd-glass laser (Peacock et al 1978) onto high-purity, solid, plane targets. The laser consists of a Q-switched oscillator, two preamplifiers and five amplifiers. The beam is focused using an aspheric F/1.4 Soro lens and with a pulse length of 1.8ns produces a power density of $2x10^{14}W.cm^{-2}$ on the surface of the target. The plane solid targets of Y,Nb,Zr and Mo were fabricated from high-purity metals while those of Rb and Sr were solid compressed pellets of rubidium and strontium carbonate.

The spectra were recorded using two types of crystal spectrograph. The first instrument is a "de-Broglie" curved crystal spectrograph (Peacock et al 1969) which employs a mica crystal (2d=19.884) wrapped around a cylindrical former 8cm in diameter and bent convex to the source, giving a large spectral range in the defocused mode. The crystal was placed 80cm from the source, in vacuum, and the spectra were recorded on Kodirex film placed inside a film cassette in the form of a segment of an outer concentric cylinder, having a broad aperture covered with a 2μm polycarbonate film and coated with 1500Å of aluminium. Twenty to thirty discharges were required to record a spectrum. Wavelength determination was accomplished using a master dispersion curve, drawn up from CuKαβ lines reflected in twelve orders from the mica crystal, with the spectrograph placed 80cm from a "Phillips" spot focus X-ray tube. Normalisation onto this curve was effected by superimposing aluminium H- and He-like reference lines on the spectrum generated at the same focal spot position during each experimental run. A wavelength accuracy of better than 0.005Å was achieved using this method.

The second instrument was a plane Bragg spectrograph employing a rubidium acid phthalate (RAP) crystal placed 10cm from the plasma. The spectra were recorded using Kodirex film placed in a rectangular box cassette. Wavelengths obtained from the curved crystal instrument were used as reference lines. At this closer distance, well exposed spectra were recorded after one laser shot. The flat crystal instrument was used in the study of lower ionisation stages, obtained by defocusing the Soro lens which produced a cooler plasma.

3. RESULTS

Figure 1 shows laser produced X-ray spectra of the elements Rb(Z=37) - Mo(Z=42) and Figure 2 that of krypton from the Plasma Focus. Table 1 gives a list of observed wavelengths together with a letter key which will be used throughout the text, tables and diagrams to label the appropriate spectral features and their assigned transitions. The most prominent features are those from Ne-like ions which produce a characteristically simple spectrum corresponding to transitions from $2s^2 2p^5 3s$, $2s2p^6 3p$ and $2s^2 2p^5 3d$ configurations to the closed shell, ground state configuration $2s^2 2p^6$. Classifications of spectra of Ne-like ions of krypton to molybdenum are given in Table 2. Here, comparison is made between the measured wavelengths, previously observed wavelengths and predicted wavelengths. Identification of the transitions involved for Kr,Sr,Zr, and Mo was accomplished by comparing the observed wavelengths with ab initio calculations by Cowan (1968, 1976, Figure 3). These results were extended to Rb,Y and Nb by the use of Moseley plots. Measured wavelengths from the present work are in good agreement with previous investigations by Aglitskii et al (1975) and Burkhalter et al (1975) and the predicted wavelengths of Boiko et al (1978). These predictions are confirmed for Kr,Rb and Sr by the present measurements the wavelengths being within 0.005Å of the predicted values.

Long wavelength satellite structure accompanies the Ne-like transitions and is particularly evident to the long wavelength side of the $2p^6 - 2p^5 3d$ features. The satellite structure consists of several major peaks (Figure 3) which have previously been identified as originating from Na- and Mg-like ions (Burkhalter et al 1975). However, a detailed classification is very difficult due to the very large number of possibilities available when 3p or 3d electrons are added to the n=2 shell with an inner shell vacancy (Table 3). An attempt has been made to classify the dominant transitions contributing to each satellite peak. The peak wavelength values of Kr,Sr,Zr, and Mo have been compared with the calculations of Cowan of the atomic structures and oscillator strengths (gf-values) of the Na-like satellites to the Ne-like transitions. By defocusing the lens in the target chamber the plasma temperature was reduced and the relative intensity of the satellite to the Ne-like structure is increased, facilitating a more positive identification of the lower ionisation stages. Figure 4 shows X-ray spectra from niobium recorded during both "hot" and "cold" plasma conditions together with a letter key assignment for these satellites. Comparison of the observed and calculated wavelengths is given in Table 3. The calculated values and

their respective oscillator strengths are given for Kr,Sr,Zr and Mo and these results were extended to Rb,Y and Nb by isoelectronic interpolation. The wavelength values for Rb,Y and Nb are listed in Table 1 opposite the appropriate letter key. The most intense structure occurs to the long wavelength side of the $2p^6 - 2p^5 3d$ transitions (Figure 3). Satellites "e" and "f" are unresolved for Kr,Rb and Mo; however, they can be distinguished for the remaining elements (Table 1). Peak "L" has been identified previously as the Ne-like transition $[2p^6]_0 - [2p^5(^2P_{3/2})3d(^2D_{3/2})]_1$ (Burkhalter et al 1975, Boiko et al 1978). However, at relatively low plasma temperatures it is likely to be heavily blended with several Na-like satellites. Burkhalter classifies feature "m" as a Mg-like satellite and as it increases in intensity at lower plasma temperatures and there are no Na-like satellites with significant oscillator strengths coincident with the measured wavelength, this assignment appears to be correct. The satellite features "o" and "r" (Figure 4) consist of bands approximately 0.02Å broad, the central wavelength values of which are given in Table 1. These features are generally lower in intensity than the rest of the satellite structure, disappearing altogether at high plasma temperatures. Burkhalter classifies these as originating from the transitions $2p^6 3s - 2p^5 3s^2$ and overlapping 3p satellites but notes a discrepancy between the calculated and experimental wavelengths. Our results show a similar discrepancy. There are however, a sufficient number of satellites with lower levels $2p^6 3d$ and $2p^6 3p$ and with non-trivial oscillator strengths to account for these band structures.

4. SUMMARY

Laser and Plasma Focus produced plasmas have been employed to investigate the X-ray spectra of highly stripped ions of the elements krypton to molybdenum. The 2 - 3 transitions in the Ne-like isoelectronic sequence have been studied for these elements and new wavelengths reported for Kr,Rb and Sr. Satellite structure has been investigated and attributed to Na-like transitions in the main. These transitions are of interest in identifying impurities of the first and second long period elements in Tokamak fusion devices with metal walls and aperture limiters. Analysis of the relative intensities of the Ne-like resonance lines and their respective satellites may prove to be a useful diagnostic tool in the study of medium-Z plasmas.

ACKNOWLEDGMENTS

The authors wish to express their gratitude to A H Jones for his technical assistance and for the operation of the Nd laser. We would also like to thank M W D Mansfield, T P Hughes and our colleagues at Culham Laboratory for useful discussions during this work. One of us (H G) acknowledges the support of the Science Research Council, being in receipt of an SRC Research Studentship during the period of this work.

REFERENCES

Aglitskii E V, Boiko V A, Krokhin O N, Pikuz S A and Faenov A Ya 1975 Sov. J. Quant. Electron. Vol. 4 No. 9 1152 - 1153

Boiko V A, Faenov A Ya, and Pikuz S A 1978 J.Q.S.R.T. Vol. 19 11 - 50

Breton C, de Michelis C and Mattioli M 1978 J.Q.S.R.T. Vol. 19 367 - 379

Burkhalter P G, Reader J and Cowan R D 1977 J. Opt. Soc. Am. Vol. 67 No. 11 1521 - 1525

Burkhalter P G, Nagel D J and Cowan R D 1975 Phys. Rev. A Vol. 11 No. 3 782 - 788

Cowan R D 1968 J. Opt. Soc. Am. Vol. 58 No. 6 808 - 818

Cowan R D and Griffin D C 1976 J. Opt. Soc. Am. Vol. 66 No. 10 1010 - 1014

Hinnov E 1976 Phys. Rev. A Vol. 14 1533 - 1541

Hotston E S 3rd Int. Conf. on Plasma Surface Interaction in Controlled Fusion Devices 30 1978

Hughes T P 1975 Plasmas and Laser Light (Bristol: Adam Hilger)

Mansfield M W D, Peacock N J, Smith C C, Hobby M G, and Cowan R D 1978 J. Phys. B: Atom. Molec. Phys. Vol 11 No. 9 1521 - 1544

Peacock N J 1977 Proc. 13th Int. Conf. on Phen. in Ionised Gases, Berlin (in Press)

Peacock N J, Galanti M, Jones A H and Lawson K D 1978 (to be published)

Peacock N J, Speer R J and Hobby M G 1969 J. Phys. B: Atom. Molec. Phys. Vol. 2 798 - 810

Pye J P, Evans K D and Hutcheon R J 1977 Mon. Not. R. astr. Soc. Vol. 178 611 - 618

Schwob J L, Klapisch M, Schweitzer N, Finkenthal M, Breton C, de Michelis C and Mattioli M 1977 Phys. Lett. Vol. 62A No. 2 85 - 89

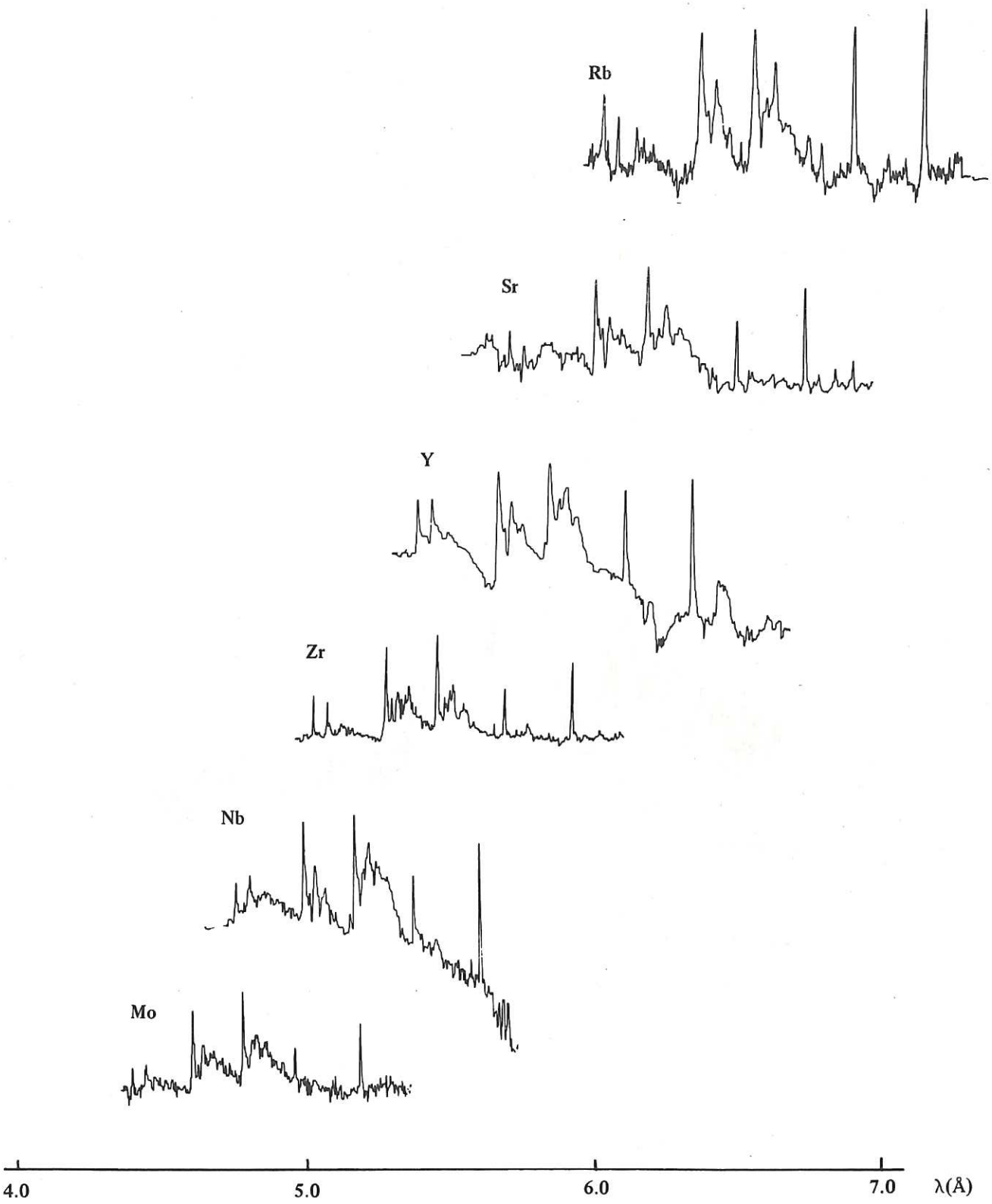

Fig.1 Laser produced X-ray spectra of Rb (Z = 37) – Mo (Z = 42) recorded using a convex curved crystal spectrograph in the de-Broglie configuration.

CLM-P550

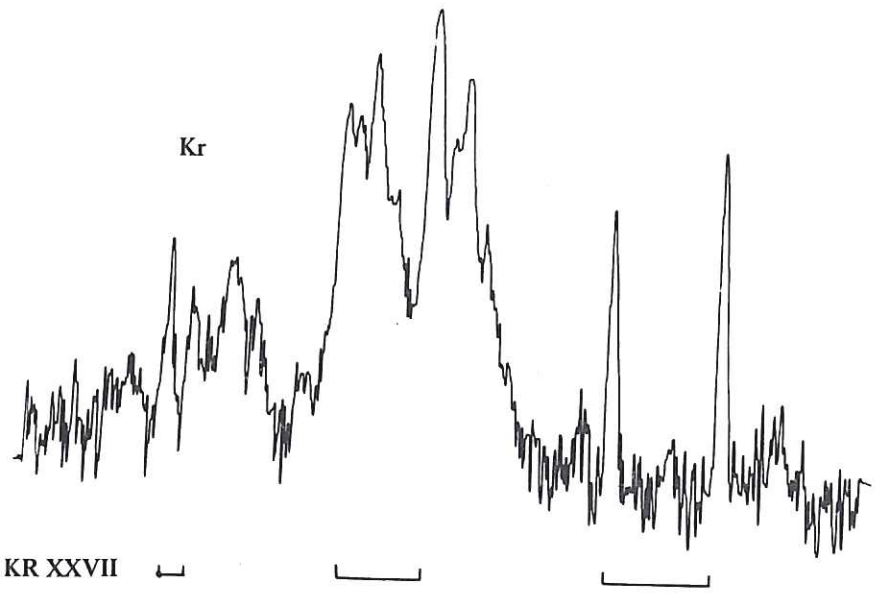

Fig.2 Resonance lines of Ne-like krypton with long wavelength satellite structure observed using a curved mica crystal spectrograph attached to the plasma focus.

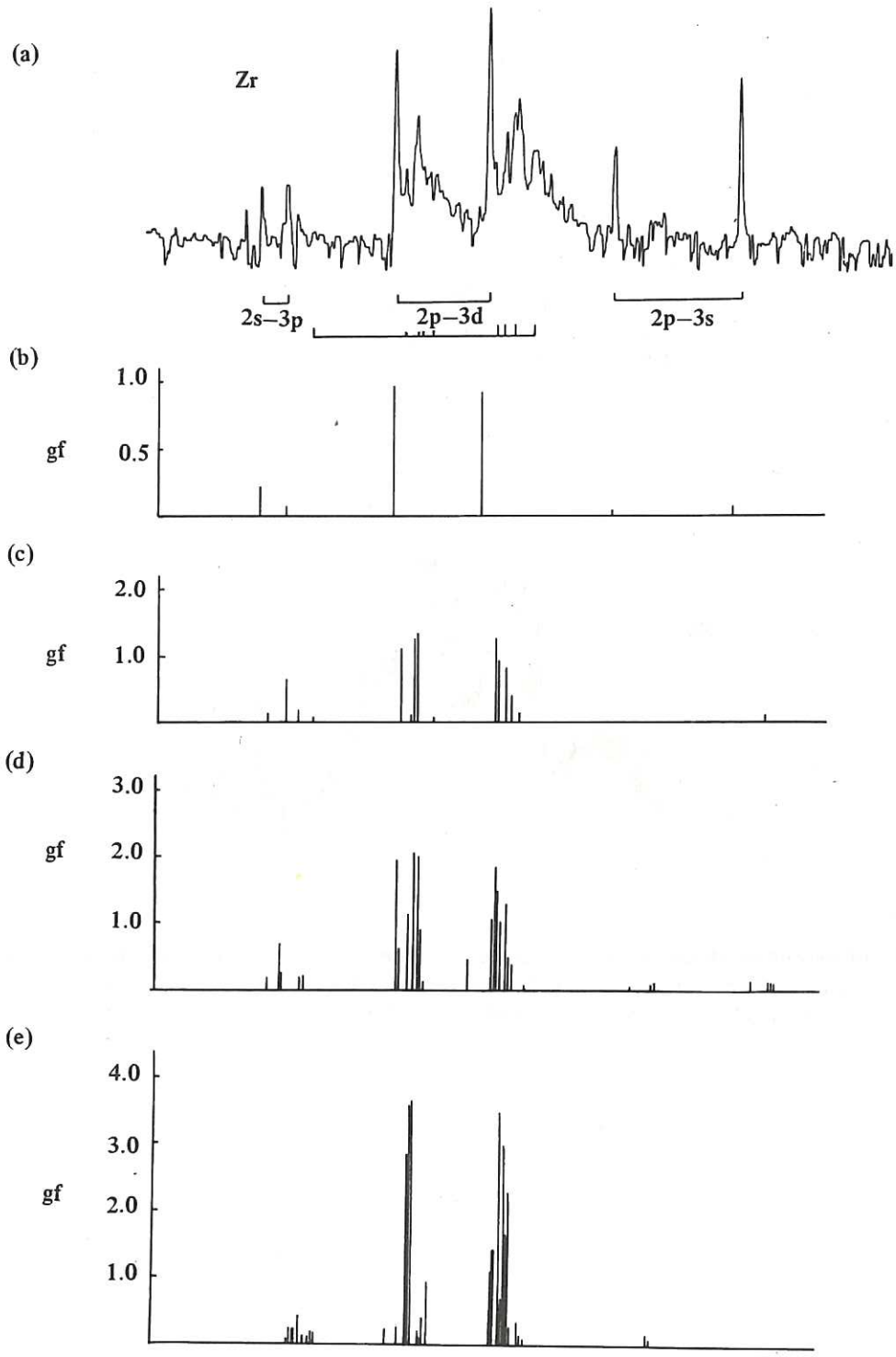

Fig.3 Comparison between observed (a) and calculated spectra for Zirconium, showing Ne-like transitions (b) and their long wavelength satellites with their lower levels $2p^63s$ (c) $2p^63p$ (d) and $2p^63d$ (e).

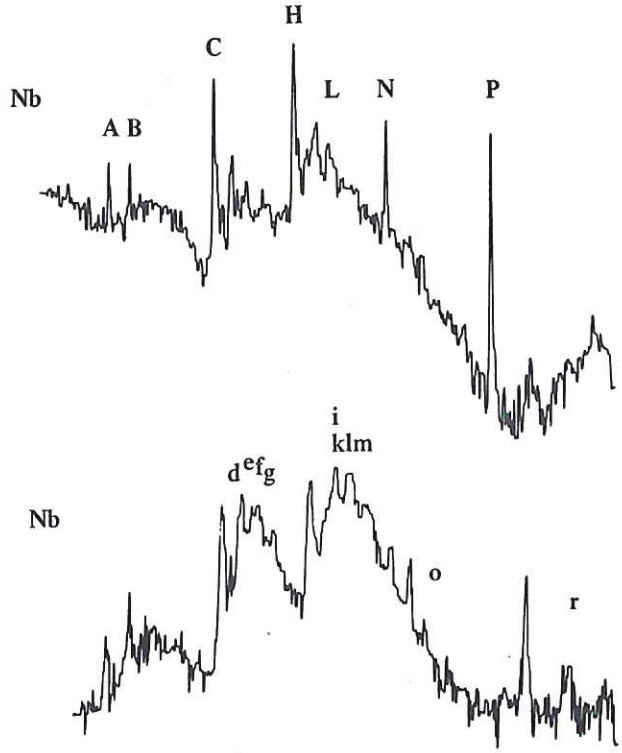

Fig.4 Comparison of Nb spectra observed using (a) a curved crystal spectrograph (b) a flat crystal spectrograph. The lower electron temperature of (b) is evident from the relative increase in intensity of the satellite structure compared with (a). Annotations A B C etc are given in the text.

Table 1 Observed Wavelengths for elements with Z=36 - 42 ($\delta\lambda \leq 0.005$Å)

Key	Element (Å)	Kr λ	Rb λ	Sr λ	Y λ	Zr λ	Nb λ	Mo λ	Ion
A		6.333	5.938	5.578	5.251	4.941	4.669	4.415	Ne-like
B		6.383	5.988	5.627	5.299	4.989	4.718	4.461	Ne-like
C		6.694	6.268	5.879	5.525	5.194	4.901	4.629	Ne-like
d		6.721	6.290	5.905	5.548	5.213	4.921	4.646	Na-like
e		6.756	6.324	5.928	5.567	5.231	4.934	4.663	Na-like
f				5.935	5.579	5.240	4.942		Na-like
g		6.801	6.361	5.971	5.600	5.270	4.971	4.689	Na-like
H		6.878	6.448	6.059	5.702	5.370	5.077	4.803	Ne-like
i		(6.924)	6.492	6.093	5.732	5.402	5.102	4.827	Na-like
k		6.931	6.508	6.103	(5.746)	5.418	5.114	4.838	Na-like
L, l		6.955	6.519	6.122	5.759	5.423	5.128	4.852	Ne/Na-like
m		6.995	6.560	6.157	5.789	5.452	5.153	4.874	Mg-like
N		7.268	6.789	6.360	5.966	5.602	5.280	4.980	Ne-like
o		7.381	(6.894)	6.457	6.052	5.683	5.357	5.047	Na-like
P		7.504	7.024	6.590	6.196	5.831	5.506	5.204	Ne-like
r		7.623	(7.135)	6.696	6.286	5.917	5.584	5.277	Na-like

Note: Wavelengths given in parentheses are not observed but a predicted value is given which is based on isoelectronic extrapolation

Table 2. Classification of spectra from Ne-like ions of elements with Z=36 - 42

			KrXXVII			RbXXVIII			SrXXIX		
			(i)	(iii)	(iv)	(i)	(ii)	(iv)	(i)	(iii)	(iv)
				(Å)			(Å)			(Å)	
Key	Classification	I	λobs	λcalc	λcalc	λobs	λcalc	λcalc	λobs	λcalc	λcalc
P	$[2s^2 2p^6]_0 - [2p^5(^2P_{3/2})3s]_1$	9	7.504	7.498	7.499	7.024	7.024	7.020	6.590	6.585	6.587
N	$-[2p^5(^2P_{1/2})3s]_1$	6	7.268	7.272	7.265	6.789	6.790	6. 788	6.360	6.365	6.357
L	$-[2p^5(^2P_{3/2})3d(^2D_{3/2})]_1$	7	6.955	6.953	6.957	6.519	6.517	6.521	6.122	6.122	6.125
H	$-[2p^2(^2P_{3/2})3d(^2D_{5/2})]_1$	10	6.878	6.874	6.878	6.448	6.447	6.449	6.059	6.054	6.058
C	$-[2p^5(^2P_{1/2})3d(^2D_{3/2})]_1$	8	6.694	6.699	6.694	6.286	6.265	6.267	5.879	5.883	5.878
B	$-[2s2p^6 3p(^2P_{1/2})]_1$	5	6.383	6.379	6.383	5.988	5.986	5.988	5.627	5.626	5.628
A	$-[2s2p^6 3p(^2P_{3/2})]_1$	4	6.333	6.332	6.334	5.938	5.936	5.939	5.578	5.580	5.580

Code

(i) Based on measurements for the present paper

(ii) Resulting from calculations using Moseley Plots

(iii) Calculations by Cowan

(iv) From Boiko et al (1978)

(v) From Burkhalter et al (1975)

I Experimental Intensity (uncorrected)

YXXX			ZrXXXI				NbXXXII			MoXXXIII		
(i)	(iv)	(ii)	(i)	(iv)	(v)	(iii)	(i)	(iv)	(ii)	(i)	(iv)	(iii)
	(Å)			(Å)				(Å)			(Å)	
λobs	λobs	λcalc	λobs	λobs	λobs	λcalc	λobs	λobs	λcalc	λobs	λobs	λcalc
6.196	6.196	6.195	5.831	5.831	5.83	5.830	5.506	5.502	5.506	5.204	5.202	5.199
5.966	5.966	5.963	5.602	5.609	5.61	5.615	5.280	5.278	5.278	4.980	4.980	4.989
5.759	5.763	5.759	5.423	5.431	5.43	5.432	5.128	5.134	5.127	4.852	4.847	4.853
5.702	5.710	5.700	5.370	5.373	5.37	5.372	5.077	5.077	5.076	4.803	4.804	4.799
5.525	5.527	5.520	5.194	5.198	5.20	5.206	4.901	4.903	4.900	4.629	4.630	4.636
5.299	5.299	5.293	4.989	4.997	5.00	4.996	4.718	4.721	4.715	4.461	4.464	4.465
5.251	5.251	5.245	4.941	4.950	4.95	4.951	4.669	4.674	4.668	4.415	4.416	4.420

Table 3 Classification of 2 - 3 spectra from Na-like ions for elements with Z = 36 - 42

key	elements				transition (jj-notation)	gf-values				intensity
	Kr	Sr	Zr	Mo		Kr	Sr	Zr	Mo	I_{exp}
	λobs	λobs	λobs	λobs		gf	gf	gf	gf	
d	6.721	5.905	5.213	4.646						4
	λcalc	λcalc	λcalc	λcalc						
	6.727	5.907	5.226	4.654	$[2p^6 3p]_{3/2} - [2p^5(^2P_{1/2})3p(^2P_{3/2})3d(^2D_{3/2})]_{5/2}$	1.714	1.872	1.952	1.968	
	6.722	5.901	5.219	4.646	$[2p^6 3s]_{1/2} - [2p^5(^2P_{1/2})3s3d(^2D_{5/2})]_{3/2}$	1.311	1.215	1.111	0.997	
	λobs	λobs	λobs	λobs						
e	6.756	5.928	5.231	4.663						6
	λcalc	λcalc	λcalc	λcalc						
	6.758	5.932	5.245	4.669	$[2p^6 3d]_{5/2} - [2p^5(^2P_{1/2})3d^2(^1G_4)]_{7/2}$	3.718	3.679	3.635	3.585	
	6.751	5.926			$[2p^6 3d]_{3/2} - [2p^5(^2P_{1/2})3d^2(^3F_2)]_{3/2}$	2.952	2.973			
			5.241	4.665	$[2p^6 3d]_{3/2} - [2p^5(^2P_{1/2})3d^2(^1D_2)]_{3/2}$			2.874	2.466	
	6.750	5.926	5.241	4.666	$[2p^6 3d]_{5/2} - [2p^5(^2P_{1/2})3d^2(^3P_1)]_{3/2}$	2.129	2.180	2.205	2.211	
	6.755	5.929	5.244	4.669	$[2p^6 3s]_{1/2} - [2p^5(^2P_{1/2})3s3d(^2D_{3/2})]_{1/2}$	1.392	1.196	1.258	1.261	
	6.755	5.930	5.244	4.668	$[2p^6 3p]_{3/2} - [2p^5(^2P_{1/2})3p(^2P_{3/2})3d(^2D_{3/2})]_{1/2}$	1.042	1.007	0.996	0.999	
	6.753	5.927	5.241	4.665	$[2p^6 3p]_{1/2} - [2p^5(^2P_{1/2})3p(^2P_{1/2})3d(^2D_{3/2})]_{1/2}$	0.759	1.129	1.145	1.147	
	λobs	λobs	λobs	λobs						
f		5.935	5.240							6
	λcalc	λcalc	λcalc	λcalc						
	6.763	5.936	5.250	4.674	$[2p^6 3d]_{5/2} - [2p^5(^2P_{1/2})3d^2(^3F_3)]_{5/2}$	4.132	3.903	3.688	3.424	
	6.759	5.934	5.248	4.671	$[2p^6 3p]_{3/2} - [2p^5(^2P_{1/2})3p(^2P_{3/2})3d(^2D_{3/2})]_{3/2}$	2.121	2.196	2.166	2.118	
	6.769	5.940	5.252	4.674	$[2p^6 3s]_{1/2} - [2p^5(^2P_{1/2})3s3d(^2D_{3/2})]_{3/2}$	1.341	1.327	1.339	1.378	
	6.764	5.936	5.249	4.672	$[2p^6 3d]_{3/2} - [2p^5(^2P_{1/2})3d^2(^3P_0)]_{1/2}$	0.703	0.699	0.704	0.714	
	λobs	λobs	λobs	λobs						
g	6.801	5.971	5.270	4.689						5
	λcalc	λcalc	λcalc	λcalc						
	6.807	5.973	5.280	4.698	$[2p^6 3d]_{3/2} - [2p^5(^2P_{1/2})3d^2(^3F_2)]_{5/2}$	1.032	0.987	0.956	0.932	
	6.791	5.959	5.270	4.681	$[2p^6 3p]_{3/2} - [2p^5(^2P_{1/2})3p(^2P_{3/2})3d(^2D_{5/2})]_{5/2}$	0.463	0.674	0.937	0.771	
	6.802	5.967	5.273	4.691	$[2p^6 3d]_{5/2} - [2p^5(^2P_{1/2})3d^2(^3F_4)]_{7/2}$	0.404	0.401	0.411	0.438	
	6.805	5.972	5.280	4.699	$[2p^6 3d]_{5/2} - [2p^5(^2P_{1/2})3d^2(^3F_3)]_{5/2}$	0.369	0.364	0.353	0.340	

	λobs	λobs	λobs	λobs					
i		6.093	5.402	4.827					6
	λcalc	λcalc	λcalc	λcalc					
	6.921	6.091	5.401	4.823	$[2p^6 3d]_{3/2} - [2p^5(^2P_{3/2})3d^2(^3F_4)]_{5/2}$	1.499	1.340	1.159	0.979
	6.921	6.093	5.406	4.828	$[2p^6 3d]_{3/2} - [2p^5(^2P_{3/2})3d^2(^3P_2)]_{1/2}$	1.246	1.321	1.382	1.432
	6.911	6.083	5.396	4.817	$[2p^6 3s]_{1/2} - [2p^5(^2P_{3/2})3s3d(^2D_{5/2})]_{3/2}$	1.327	1.352	1.250	1.011
	6.915	6.089	5.403	4.826	$[2p^6 3d]_{5/2} - [2p^5(^2P_{3/2})3d^2(^1S_o)]_{3/2}$	1.093	1.285	1.476	1.659
	6.922	6.095	5.408	4.831	$[2p^6 3p]_{3/2} - [2p^5(^2P_{3/2})3p(^2P_{3/2})3d(^2D_{5/2})]_{3/2}$	0.940	1.213	1.471	1.598
	6.922	6.094	5.406	4.829	$[2p^6 3p]_{3/2} - [2p^5(^2P_{3/2})3p(^2P_{3/2})3d(^2D_{5/2})]_{5/2}$	0.792	1.370	1.850	2.210
	6.915	6.088	5.401	4.824	$[2p^6 3p]_{3/2} - [2p^5(^2P_{3/2})3p(^2P_{3/2})3d(^2D_{5/2})]_{1/2}$	0.887	0.990	1.076	1.149
	6.918	6.089	5.401	4.823	$[2p^6 3s]_{1/2} - [2p^5(^2P_{3/2})3s3d(^2D_{5/2})]_{1/2}$	0.787	0.878	0.953	1.012
	λobs	λobs	λobs	λobs					
k	6.931	6.103	5.418	4.838					6
	λcalc	λcalc	λcalc	λcalc					
	6.932	6.102	5.413	4.834	$[2p^6 3d]_{5/2} - [2p^5(^2P_{3/2})3d^2(^3F_4)]_{5/2}$	2.653	3.106	3.524	3.897
	6.945	6.112	5.421	4.840	$[2p^6 3d]_{3/2} - [2p^5(^2P_{3/2})3d^2(^1G_4)]_{5/2}$	2.294	2.652	2.986	3.286
	6.940	6.109	5.419	4.840	$[2p^6 3p]_{3/2} - [2p^5(^2P_{3/2})3p(^2P_{3/2})3d(^2D_{5/2})]_{3/2}$	1.054	0.967	0.840	0.703
	6.938	6.108	5.419	4.839	$[2p^6 3d]_{5/2} - [2p^5(^2P_{3/2})3d^2(^3P_2)]_{3/2}$	0.867	0.842	0.794	0.733
	6.948	6.111	5.417	4.834	$[2p^6 3s]_{1/2} - [2p^5(^2P_{3/2})3s3d(^2D_{5/2})]_{3/2}$	0.675	0.728	0.822	0.939
	6.942	6.108	5.417	4.837	$[2p^6 3p]_{1/2} - [2p^5(^2P_{3/2})3p(^2P_{1/2})3d(^2D_{5/2})]_{1/2}$	0.517	0.787	0.992	1.088
	λobs	λobs	λobs	λobs					
l	6.955	6.122	5.423	4.852					7
	λcalc	λcalc	λcalc	λcalc					
	6.950	6.118	5.427	4.847	$[2p^6 3d]_{5/2} - [2p^5(^2P_{3/2})3d^2(^1G_4)]_{7/2}$	2.083	2.219	2.333	2.429
	6.950	6.117			$[2p^6 3d]_{3/2} - [2p^5(^2P_{3/2})3d^2(^3P_2)]_{3/2}$	1.300	1.488		
			5.425	4.844	$[2p^6 3d]_{3/2} - [2p^5(^2P_{3/2})3d^2(^3F_3)]_{3/2}$			1.668	1.837
	6.949	6.117	5.426	4.846	$[2p^6 3p]_{3/2} - [2p^5(^2P_{3/2})3p(^2P_{3/2})3d(^2D_{5/2})]_{5/2}$	1.433	1.402	1.344	1.279
	6.956	6.123	5.432	4.852	$[2p^6 3d]_{5/2} - [2p^5(^2P_{3/2})3d^2(^1G_4)]_{5/2}$	0.745	0.650	0.536	0.421
	6.960	6.121	5.426	4.842	$[2p^6 3s]_{1/2} - [2p^5(^2P_{3/2})3p^2(^1S_0)]_{3/2}$	0.104	0.223	0.386	0.631

Note : Only the largest squared eigenfunction component is listed.